0-6814-TM2

TECHNICAL MEMORANDUM

TM-1: Report of Task 2 – Material Characterization

TxDOT Project 0-6814: Performance Evaluation, Specifications, and Implementation of Non-Tracking Tack Coat

DATE: January 9, 2014

TO: Darrin Jensen (TxDOT)

COPY TO: Mary Levien (TTI)

FROM: Ah Young Seo, Graduate Research Assistant, TTI
Bryan Wilson (PI), Assoc. Research Scientist, TTI
Maryam Sakhaeifar, Ph.D., Assistant Professor, TAMU

FOR MORE INFORMATION:
Name Bryan Wilson
Phone (979) 458-7989
Email b-wilson@ttimail.tamu.edu

OVERVIEW

The purpose of this memorandum is to report on the work involved in Task 2 – *Material Characterization*. The work involved collecting and testing non-tracking tacks and a standard tack.

MATERIAL COLLECTION AND PROCESSING

The researchers contacted asphalt emulsion suppliers and requested samples of the tack materials listed in Table 1.

Table 1. Tack Materials

Product Name	Formulation Name	Supplier
Trackless Tack	NTSS-1HM	Blacklidge
Ultrafuse	-	Blacklidge
Trackless Tack	NTQS-1HH	Calumet
Fast Set	QS-1HH	Western Emulsions
eTac-H	CQS-1HT	Ergon
eTac	CBC-1LR	Ergon
Control tack	CSS-1H	Ergon

To clarify, while two products are named "Trackless Tack," the materials are not the same. Blacklidge has trademarked the name "Trackless Tack," and has licensed the name to Calumet. In return, Calumet supplies Blacklidge with neat hard-pen binder, which Blacklidge modifies to create their version of Trackless Tack. In this study, the material from Blacklidge is referred to as Trackless Tack (B), and the material from Calumet is referred to as Trackless Tack (C). Another point of confusion is related to two the eTac products. Until recently, Ergon sold a non-tracking product named eTac. Now, they are producing a similar product and have changed their naming conventions. The new product now goes by the name eTac and the original product is now called eTac-H.

New tack samples were requested on an as-need basis, and tacks stored for more than one month was not used. At this time, the research team still needs to request and test CSS-1H tack (traditional tack).

Most of the tests in this task were performed on binder residues. The residue was collected using the new 6-hr evaporative technique which is specified in AASHTO PP72 Method B. The emulsions was first stirred and then spread over a silicon mat to a thickness of 0.015 inch with a thin film applicator (Figure 1a). The mat was transferred to a flat tray, tested for correct film thickness with a wet film thickness gauge, and placed in an oven at 60 °C for 6 hours (Figure 1b). The emulsion residue left after evaporation was carefully peeled from the mat. This process was repeated until enough residue was collected for testing.

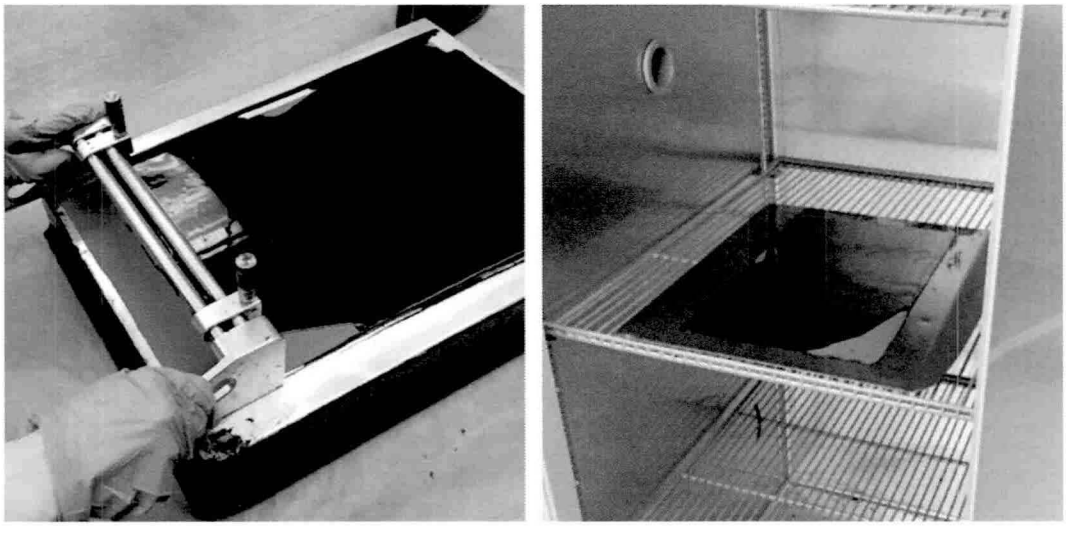

(a) **(b)**

Figure 1. Sample preparation for emulsion recovery: a) thin-film application and b) evaporation of water in oven.

CHARACTERIZATION METHODS

In this task, different properties of the tacks and tack residues were collected as summarized in Table 2. Properties from standard test types were requested from the suppliers. The properties from the three advanced tests were performed at TTI. The advanced tests include 1) frequency sweep test, 2) multiple-stress creep-recovery test, and 3) liner amplitude sweep test,

as discussed in this report. The results of all listed tests except the Liner Amplitude Sweep (LAS) test, which is still incomplete, are discussed in this task.

Table 2. Properties of residual binders and emulsions

Material Type	Property	Test Type	Test Procedures
Residue	Viscosity	Standard	AASHTO T 316
	Penetration	Standard	AASHTO T 49
	Softening point	Standard	AASHTO T 53
	Complex shear modulus ($\|G^*\|$) Phase angle (δ)	Standard/Advanced	AASHTO T 315
	Percent recovery Non-recoverable creep (J_{nr})	Advanced	MSCR test: ASTM (D7405)
	Failure strain @ max stress Cycles to failure (N_f)	Advanced	Linear Amplitude Sweep: AASHTO TP 101
Emulsion	Residue content (%)	Standard	Tex-543-C
	Saybolt viscosity	Standard	D 562

In both the frequency sweep test and multiple-stress creep-recovery (MSCR) test, unaged binders were used. Aged binders were used in the LAS test to address fatigue characteristics. Aging was done through the pressure-aging vessel (PAV) process, specified in AASTHO R 28, to simulate long-term aging during in-service life of asphalt pavements. This study did not consider the short-term aging procedure through the rolling thin-film oven (RTFO). The RTFO process is used to simulate aging of asphalt in the batching process, and therefore does not apply to emulsion (*1*). Table 3 gives the breakdown of what type of binder was used for each test.

Table 3. Matrix for Advanced Tests*

Tack Type	Residue Binder	Neat Binder
eTac-H	✓	
eTac	✓	✓
Trackless Tack (B)	✓	✓
Ultrafuse		✓
Fast Set	✓	
Trackless Tack (C)	✓	

* Unaged binders used for the frequency sweep and MSCR tests.
PAV aged binders used for the LAS test.

DSR Frequency Sweep

The frequency sweep test was conducted to identify the undamaged rheological properties of asphalt binder by applying constant loading with low amplitude. The test is run over a wide range of loading frequencies at multiple temperatures using the dynamic shear rheometer. In this test, the absolute value of the complex shear modulus, $|G^*|$, and the phase angle, δ, of the asphalt binder are measured. Emulsion residues, cured through AASHTO PP72 Method B, as well as their neat binders were tested as well. The range of loading frequencies is from 1 to 100 rad/s. **Error! Reference source not found.** shows the selected temperatures, plate geometries and the strain level applied in this study. The test temperature was stabilized in a

forced air chamber. The 25-mm parallel plates with a 1.0 mm gap were used at high temperatures, and the 8-mm parallel plates with a 2.0 mm gap were used at intermediate temperatures.

Table 4. DSR test conditions

Temperature (°C)	DSR plate	Strain level
6	8-mm	0.1~0.2
10		
22		
34		
46	25-mm	1~5
58		
70		

A master curve was created based on a time-temperature superposition concept and the assumption of thermorheologically simple materials (*2*). Figure 2 shows the desired master curve. As shown in Figure 2 (a), the resulting data at three temperatures are plotted versus loading frequency. In this case, T_2 was selected as a reference temperature, and the data at the lower temperature, T_1, were shifted to a higher frequency, and the data of the higher temperature, T_3, were shifted to a lower frequency. This forms the single curve, Figure 2 (b), of the complex shear modulus versus the reduced frequency in logarithmic scale. The reduced frequency means the computed frequency at the reference temperature equals the actual loading frequency at the desired temperature (*3*). The reduced frequency can be expressed as follows:

$$f_r = f \times a(T_i) \tag{1}$$

where,

$a(T_i)$ = shift factor as a function of temperature
T_i = temperature
f = loading frequency at desired temperature
f_r = reduced loading frequency at reference temperature

Here, the shift factor forms a second order polynomial relationship in terms of temperature. The relationship is shown in Equation (2):

$$\log a(T_i) = aT_i^2 + bT_i + c \tag{2}$$

where,

$a,\ b, c$ = coefficients of the second order polynomial.

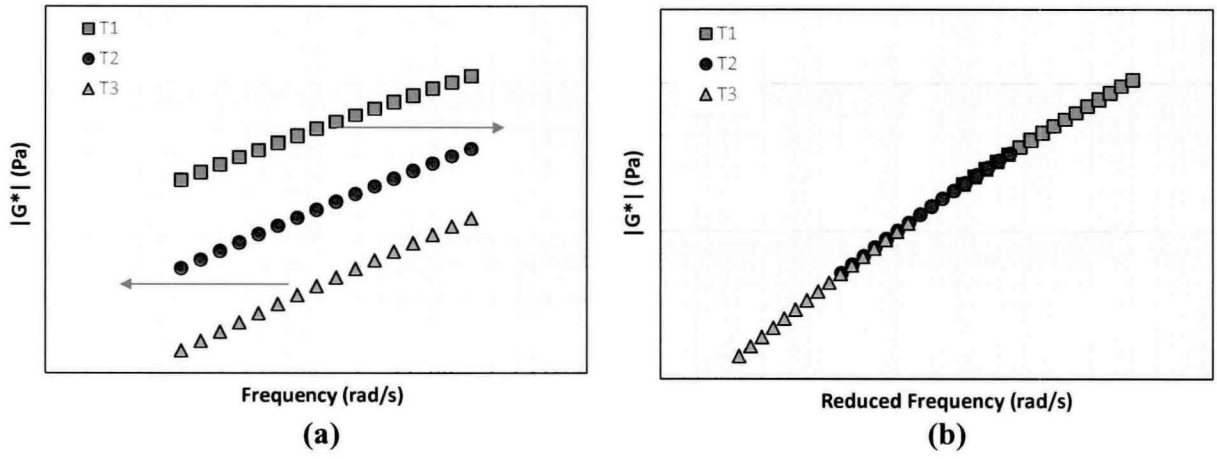

Figure 2. Construction of master curve: $|G^*|$ vs. frequency, and (b) $|G^*|$ vs. reduced frequency

The master curve model used in this study is based on the Christensen-Anderson-Marasteanu (CAM) model (*4*). The equation of the CAM model is as follows:

$$\left|G^*(\omega)\right| = \mathrm{G_g}\left[1+\left(\frac{\omega_c}{\omega}\right)^v\right]^{-\frac{w}{v}} \tag{3}$$

where,

$|G^*(\omega)|$ = absolute value of complex shear modulus in terms of ω (Pa),
$\mathrm{G_g}$ = glassy modulus,
ω_c, v, w = model parameters.

The typical value of the glassy modulus is 1.0 GPa. This parameter indicates the limiting stiffness obtained at very low temperatures or high frequencies where physical hardening of viscoelastic materials is dominant. Three shift factor coefficients in Equation (2) and three model parameters in Equation (3) are simultaneously determined with the Solver tool in Microsoft Excel. The model parameters fitted to the data can be used to predict the value of complex shear modulus or phase angle at any desired temperature and frequency of loading within the range of testing conditions.

The master curves were constructed for neat binders and residues of tack materials using DSR frequency sweep data. The reference temperature for all master curves was 34 °C. Whereas the modulus mater curves seem to be smooth, the phase angle curves are expected vary with temperature.

Multiple-Stress Creep-Recovery

The MSCR test is the latest method to improve the current PG specification. This method is suggested to replace the existing dynamic shear test because of a better correlation with field performance, particularly rutting (*5*). The MSCR test has been used to investigate the effect of modification on rutting performance (*6*). Furthermore, the MSCR recovery can also indicate the fatigue resistance of asphalt binder when evaluating the elastic response (*7; 8*), thus, this study

uses the MSCR test to address the resistance to fatigue cracking in addition to rutting. The test is conducted at 60°C, which is the same temperature used in the residue recovery method. At this high temperature, the 8-mm plate geometry with 1-mm gap setting is used in the DSR.

Error! Reference source not found. shows the stress input and the strain output of a sample, as specified in ASTM D7405. In this test, a one-second creep load is applied to the sample resulting in an increase in strain. After each loading cycle, the load is removed and the sample is allowed to recover for 9 seconds, however the sample is not able to return to the unloaded state. A portion of strain is recovered, and the rest remains as non-recoverable strain. The MSCR test procedure involves two sets. A low stress level of 0.1 kPa is applied for 10 cycles in the first set, and a high stress level of 3.2 kPa is loaded for 10 cycles in the next set. As the loading cycles increase at different stress levels, the non-recoverable strain is accumulated, representing the potential of permanent deformation in pavement.

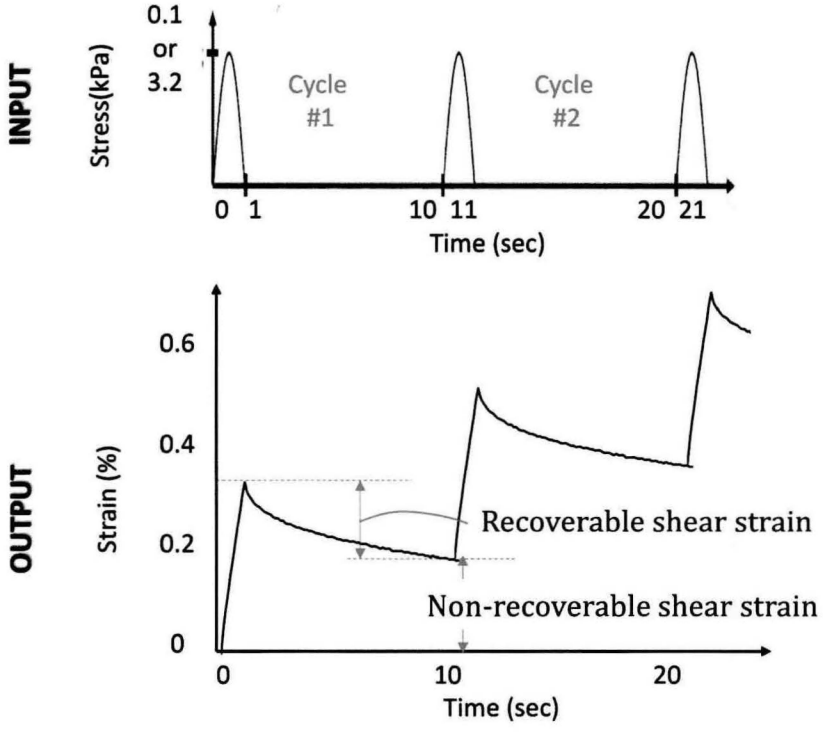

Figure 3. Input and output of MSCR test

The parameters determined by the MSCR test are the average percent recovery and the non-recoverable creep compliance. The percent recovery is defined as the delayed elastic response of a binder and calculated as the following equation:

$$\%\text{Recovery} = \frac{\gamma_r}{\gamma_p} \times 100 \tag{4}$$

where,

γ_r = recoverable shear strain

γ_p = peak shear strain.

The non-recoverable creep compliance (J_{nr}) represents the residual strain after repeated loading with respect to the stress level. The J_{nr} is a parameter representing the resistance to permanent deformation under repeated loading. The non-recoverable creep compliance is determined using Equation (5):

$$J_{nr} = \frac{\gamma_u}{\tau_{Applied}} \tag{5}$$

where,

γ_u = non-recoverable shear strain

$\tau_{Applied}$ = applied shear stress.

These parameters are used to assess the material properties of the binder related to the fatigue resistance as well as the rutting resistance. The MSCR data will be analyzed and illustrated in the result section.

Liner Amplitude Sweep

The LAS test is the advanced method for characterizing the fatigue resistance of asphalt binder. This test was developed to compensate for the limitation of the existing PG specification. Since the properties of the binder in the existing specification are within a linear viscoelastic range, the specification is deficient to predict the actual fatigue life (*9*). Moreover, the existing PG fatigue parameter is measured at only a few loading cycles and one strain level so that the impact of traffic and pavement structure on the fatigue resistance is neglected (*10*).

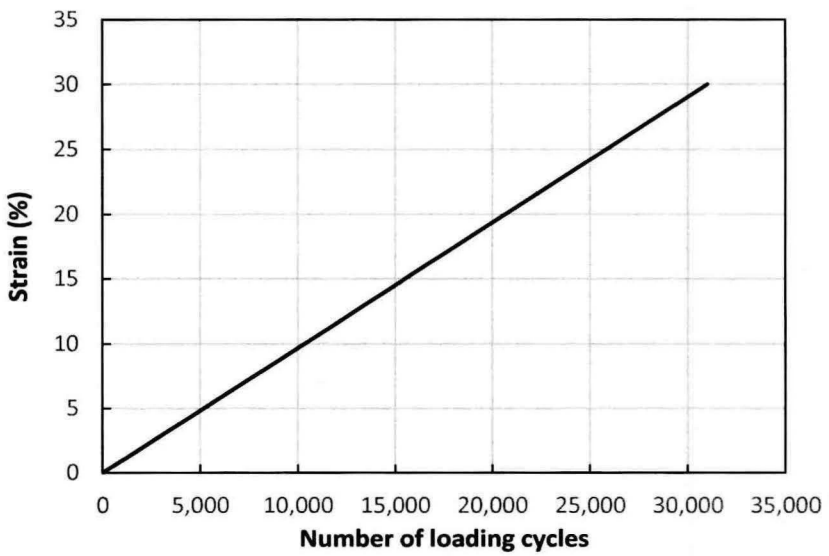

Figure 4. Loading scheme for amplitude sweep test in AASHTO-TP101

The LAS test procedure involves a frequency sweep test and an amplitude sweep test. First, the frequency sweep test investigates the rheological properties of undamaged material. This test is conducted at constant strain amplitude over various loading frequencies. The strain level is 0.1percent, and twelve loading frequencies are applied: 0.2, 0.4, 0.6, 0.8, 1.0, 2.0, 4.0,

6.0, 8.0, 10, 20, and 30 Hz. The amplitude sweep identifies the characteristic of fatigue damage. It is performed using oscillatory loading in a strain-controlled mode at a constant frequency of 10 Hz, and is accelerated by applying a linearly increasing load. Figure 4 shows a loading scheme for amplitude sweep test in AASHTO-TP101. The loading step consisting of 100 cycles increasing at 0.1percent strain from 0.1 to 30 percent applied strain.

Two tests in the LAS test procedure are run using the DSR at the selected temperature. In DSR testing, the 8-mm parallel plate geometry with a 2-mm gap was used. The temperature is determined as where the fatigue parameter ($|G^*| \cdot sin\delta$) reaches the current PG specification limit of 5.0 GPa (*11*).

To analyze the LAS test results, the viscoelastic continuum damage concept was used to calculate the fatigue resistance of the sample. The damage growth in viscoelastic materials is defined as the change in the energy potential (W) relative to the change in the damage intensity (D), following the Paris' Law suggested by Schapery (*12*), as shown in Equation (6):

$$\frac{dD}{dt} = \left(-\frac{\partial W}{\partial D}\right)^{\alpha} \tag{6}$$

where

α = energy release rate ($=1/m$);
W = work potential;
D = damage intensity; and
t = time.

The parameter α can be obtained using m-value which is the slope of a storage modulus versus angular frequency curve on logarithmic scale. Here, the storage modulus, G′ , is in terms of at angular frequency. Thus, the frequency sweep data need to be converted into time domain by using the method of interconversion (*11*). The storage modulus is calculated using Equation (7):

$$G'(\omega) = |G^*|(\omega) \times \cos\delta(\omega) \tag{7}$$

where

ω = angular frequency (rad/s);
G' = storage modulus;
$|G^*|$ = complex shear modulus; and
δ = phase angle.

The work potential is determined using dissipated energy subjected to loading in strain-controlled mode (*13*). The dissipated energy is defined as follows:

$$W = \pi . I_D . \gamma_o^2 . |G^*| . \sin\delta \tag{8}$$

where:

W = dissipated energy;

I_D = initial undamaged value of $|G^*|$; and

γ_0 = shear strain.

The damage intensity (D) is determined by integrating Equation (6) in which Equation (8) is substituted, and becomes as follows:

$$D(t) \cong \sum_{i=1}^{N} \left[\pi I_D \gamma_o^2 \left(|G^*| \sin \delta_{i-1} - |G^*| \sin \delta_i \right) \right]^{\frac{a}{1+a}} (t_i - t_{i-1})^{\frac{1}{1+a}} \tag{9}$$

The material parameter $|G^*| \sin \delta$ is plotted against the damage intensity D, and the following relationship is fitted to experimental data.

$$|G^*| \sin \delta = C_0 - C_1 (D)^{C_2} \tag{10}$$

where,

C_0, C_1 and C_2 = model coefficients.

Equation (10) can be substituted into Equation (8) and then the derivative of the dissipated energy in Equation (8) can be determined with respect to the damage intensity D. The equation yields as follows:

$$\frac{dW}{dD} = \pi I_D C_1 C_2 (D)^{C_2 - 1} (\gamma_{max})^2 \tag{11}$$

Once Equation (11) is substituted into Equation (6), it is integrated to obtain the relationship of the number of cycles to failure N_f and the strain amplitude γ_{max}. The simplified relation is the following equation:

$$N_f = A(\gamma_{max})^{-2\alpha} \tag{12}$$

where,

$$A = \frac{f(D_f)^k}{k(\pi C_1 C_2)^{\alpha}} \tag{13}$$

$k = 1 + (1 - C_2)\alpha$; and

D_f = damage accumulation at failure.

Using Equation (12), one can determine the fracture life at any strain level under a given damage intensity. Hence, the LAS test enables the prediction of the fatigue resistance under various conditions (*10*).

CHARACTERIZATION RESULTS

DSR Frequency Sweep

Figure 5 shows the master curve for the neat binder and the residue of eTac. As shown in Figure 5 (a), the stiffness of the residue is higher than that of the neat binder. It indicates that multiple factors involving addition of emulsifying agent and aging in recovery procedure cause the emulsion residue to harden. This effect, however, is not applicable at high frequency or low temperature. Figure 5 (b) presents the decrease in phase angles of the residue, which indicates the residue became more elastic than the neat binder. For both binders, the sudden reduction in the phase angle occurs at low frequency or high temperature.

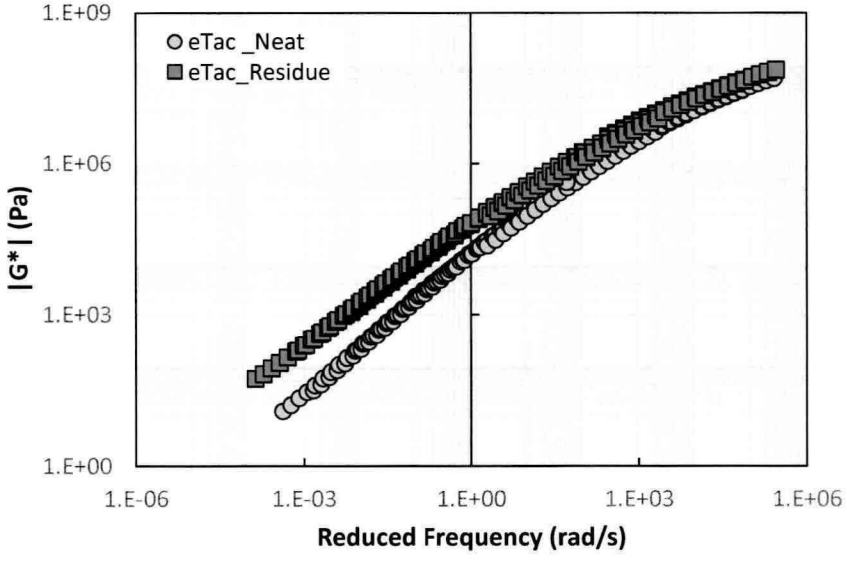

(a)

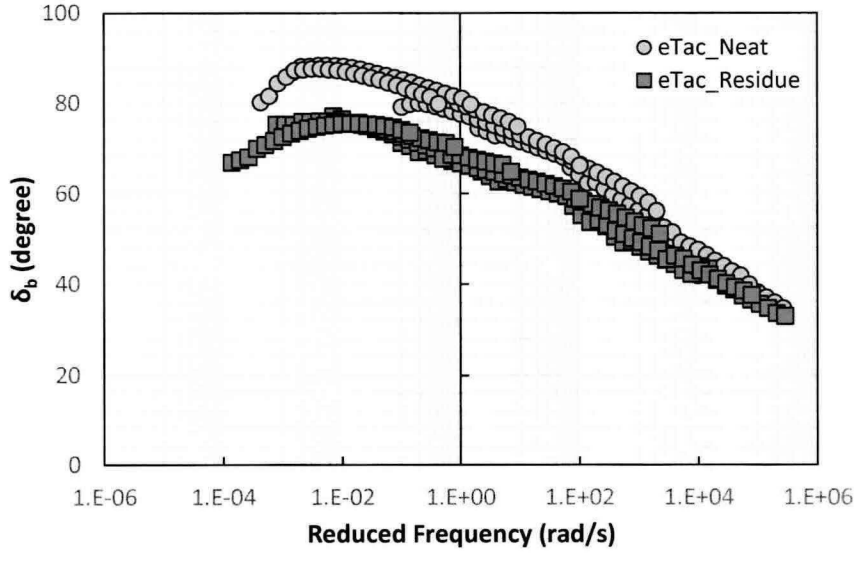

(b)

Figure 5. Master curve for neat binder and residue of eTac: (a) complex shear modulus, and (b) phase angle

Figure 6 shows the master curve for the neat binder and the residue of Trackless Tack manufactured by Blacklidge. In Figure 6 (a), the residue becomes stiffer than the neat binder over the entire range of frequency. As the frequency decreases, the difference in stiffness between the residue and the neat binder of Trackless Tack (B) is greater than those of eTac. It may be caused by the type of emulsifying agents or water/asphalt content in the materials. The more water is contained in emulsions, the thinner layer of the residue generates, which provides more aging during recovery. Figure 6 (b) shows more elastic behavior of the residue than the neat binder. The slope of phase angles for the residue remains constant even at low frequency or high temperature, unlike the neat binder.

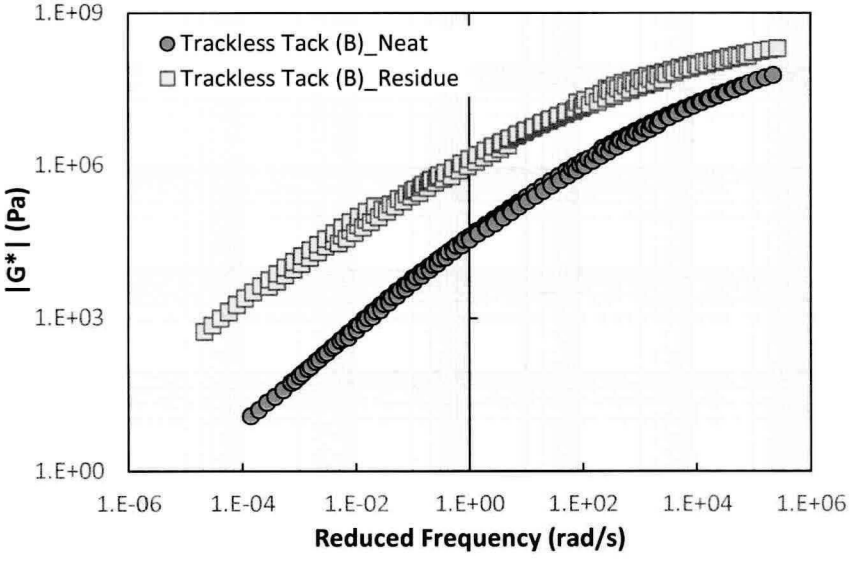

(a)

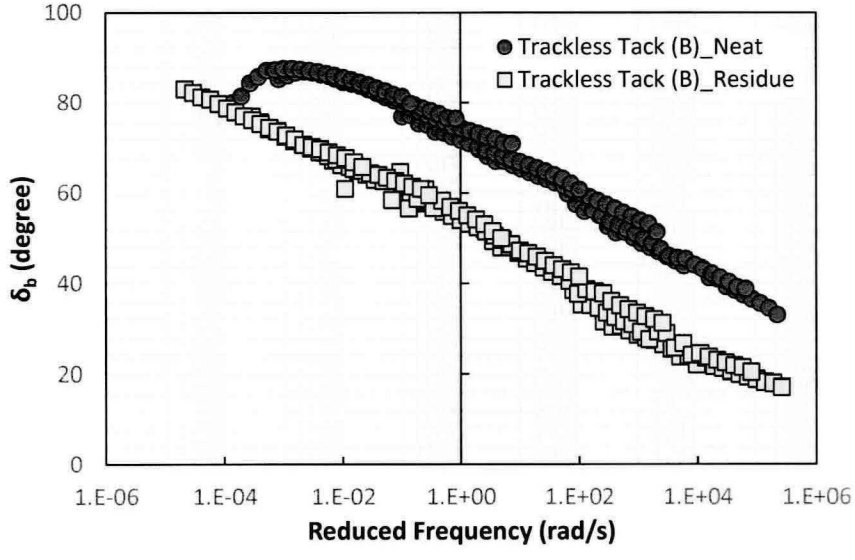

(b)

Figure 6. Master curve for neat binder and residue of Trackless Tack (Blacklidge): (a) complex shear modulus, and (b) phase angle

Figure 7 shows the master curves of all emulsions together. The eTac and eTac-H exhibit similar stiffness values with frequency, but eTac has slightly lower phase angle at low frequencies than eTac-H. Trackless Tack (B) residue is the stiffest material. Also, the slope of the stiffness curve seems to be flat, which indicates the residue is less susceptible to the change in frequencies or temperatures. Both Trackless Tack (B) and (C) have higher modulus values at low frequency than other residues. However, Trackless Tack (C) is more viscous at low and intermediate frequencies since high phase angle corresponds to more viscous and less elastic material. The Ultrafuse exhibits the same rheological properties as Trackless Tack (B). FastSet belongs to the middle rank with respect to the stiffness, but becomes more viscous than other residues, especially at low frequency or high temperature.

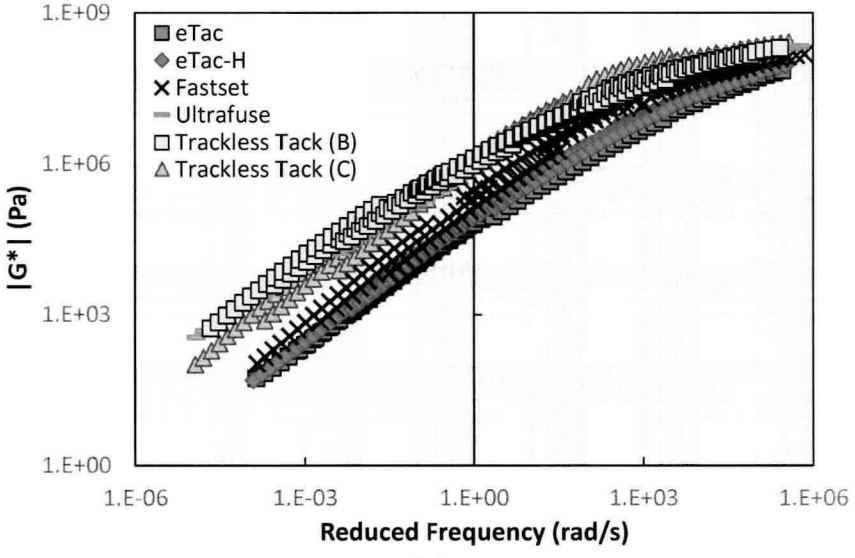

(a)

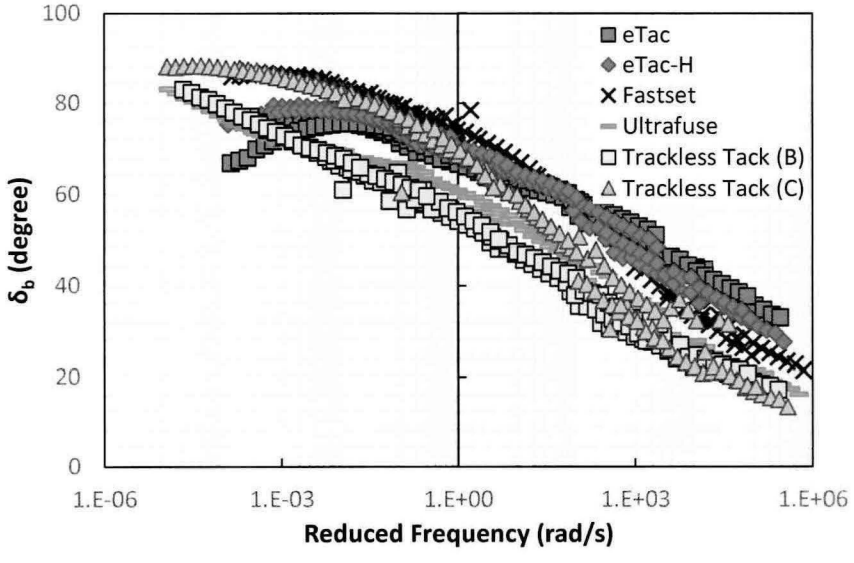

(b)

Figure 7. Master curve for non-tracking tack coat materials: (a) complex shear modulus, and (b) phase angle

Error! Not a valid bookmark self-reference. presents the coefficients of shift factor and the model parameters fitted to the modulus data to predict the properties at various testing conditions. Using these coefficients and parameters, the rheological properties of the residues and the neat binders at 60 °C and 10 rad/s are determined and ranked as shown in **Error! Not a valid bookmark self-reference.**Table 6.

Table 5. Coefficients of shift factor and model parameters

Binder Type		*a*	*b*	*c*	ω_c	υ	*w*
eTac-H	Residue	0.000692	-0.153	4.397	0.224	0.0609	1.53
eTac	Neat	0.000876	-0.157	4.328	0.237	0.0638	1.77
	Residue	0.000683	-0.151	4.328	2.389	0.0610	1.41
Trackless Tack (B)	Neat	0.000624	-0.144	4.183	0.181	0.0623	1.67
	Residue	0.000313	-0.134	4.210	0.171	0.0572	1.22
Ultrafuse	Neat	0.000396	-0.150	4.652	2.20	0.0590	1.14
Fast Set	Residue	0.000389	-0.143	5.233	2.18	0.0666	1.44
Trackless Tack (C)	Residue	0.000282	-0.139	4.393	0.105	0.0650	1.44

Table 6. Predicted rheological properties at 60 °C and 10 rad/s

Binder Type		|G*| (kPa)	Rank *	δ(°)	Rank*
eTac-H	Residue	8.495	*E*	71.98	*C*
eTac	Neat	7.05	*F*	70.46	*E*
	Residue	2.32	*H*	81.48	*A*
Trackless Tack (B)	Neat	3.33	*G*	77.788	*B*
	Residue	91.9	*A*	58.45	*H*
Ultrafuse	Neat	58.6	*B*	59.28	*G*
Fast Set	Residue	36.3	*D*	70.87	*D*
Trackless Tack (C)	Residue	42.01	*C*	69.42	*F*

* *Note*: The highest ranking is denoted as "*A*", and lowest one is "*H*"

Multiple-Stress Creep-Recovery

The average percent recovery represents the amount of recovery in strain after unloading. A high percent recovery represents higher level of elasticity contribution, thereby resulting in better performance against rutting and fatigue cracking (*8*). Figure 8 presents the average percent recovery for the residue of Trackless Tack (B) and eTac and their neat binders at two different stress levels of 0.1 kPa and 3.2 kPa. The residue shows higher percent recovery than the neat binder for both tacks. It is observed that the percent recovery of the neat binder approaches zero, indicating that the elasticity in the neat binder hardly contributes to the recovery.

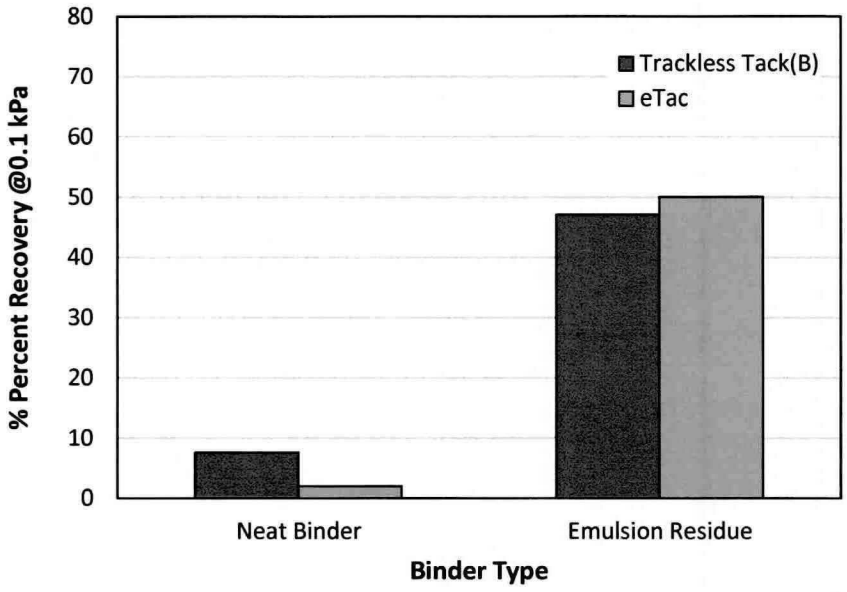

(a)

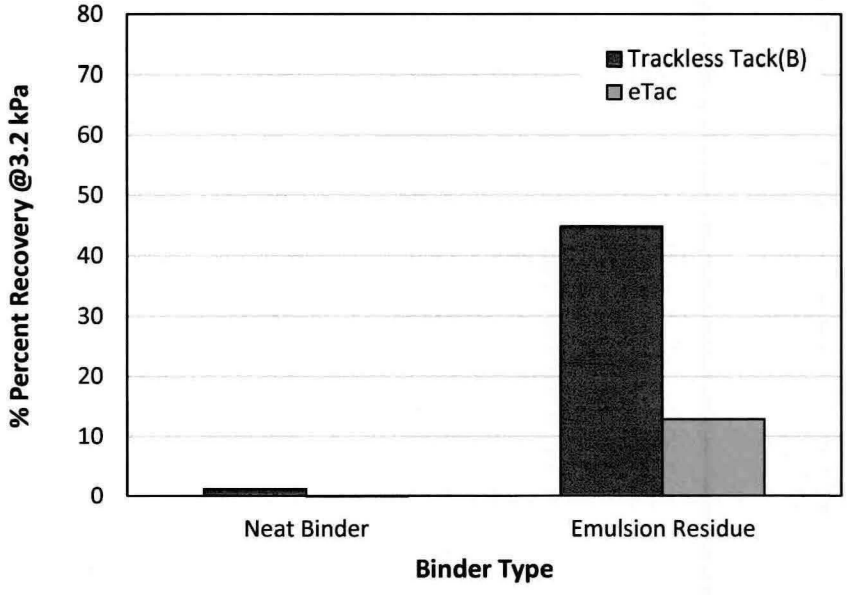

(b)

Figure 8. Percent recoevery at different stress levels of emulsion residues and their neat binders; (a) 0.1 kPa and (b) 3.2 kPa

Figure 9 displays the results on non-recoverable creep compliance (J_{nr}) of the neat binder and the residue for eTac and Trackless track (B) measured at 60°C and two stress levels of 0.1 kPa and 3.2 kPa. The binder with lower J_{nr} tends to be less susceptible to permanent deformation. The J_{nr} of the residue is lower than that of the neat binder for two materials. Aging and emulsification leads to the dramatic reduction in J_{nr}. Compared to Trackless Tack (B), eTac exhibits higher J_{nr} at two stress levels. This indicates that Trackless Tack (B) has higher resistance to rutting than eTac.

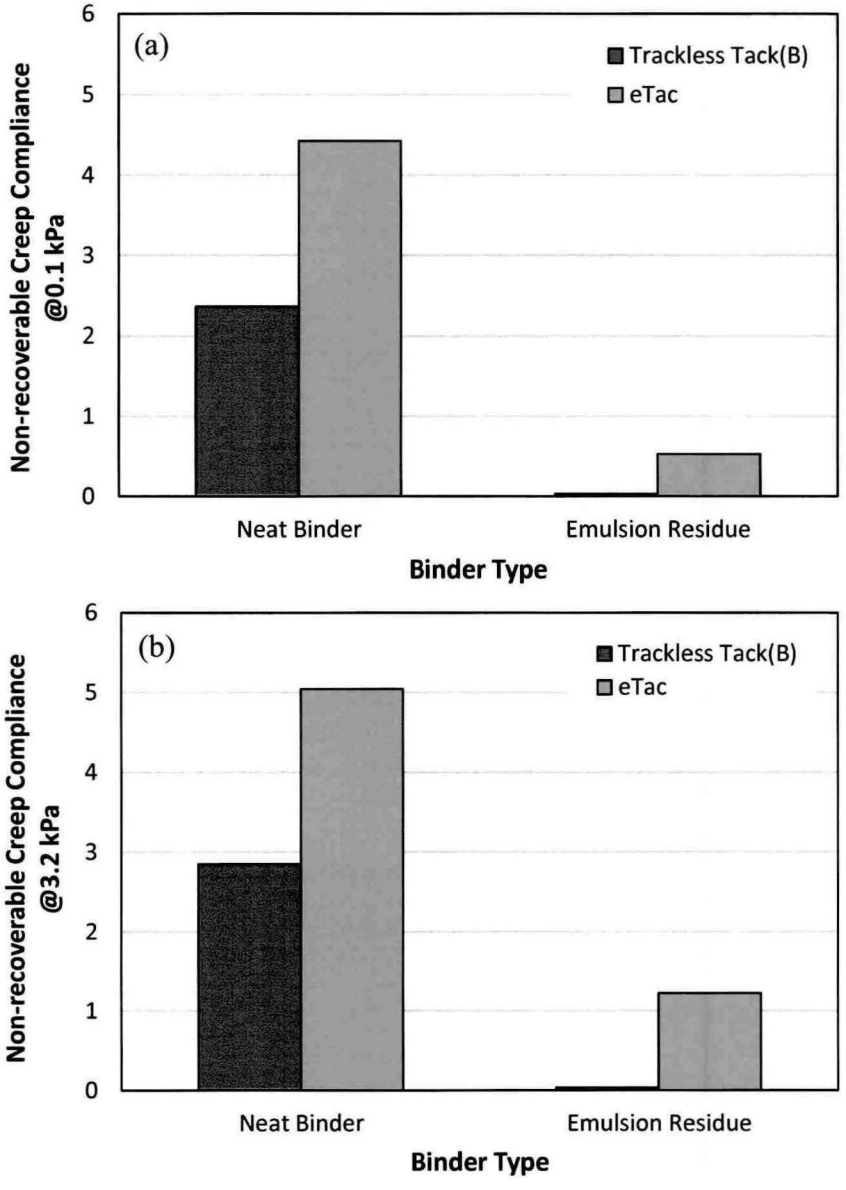

Figure 9. Non-recoverable creep compliance at different stress levels of emulsion residues and their neat binders; (a) 0.1 kPa and (b) 3.2 kPa

Figure 10 and Figure 11 present the percent recovery and non-recoverable creep complinace at different stress levels of the residue for all non-tracking tack coat materials, respectively. In Figure 10, Ultrafuse shows the highest level of recovery whereas Trackless Tack (C) has the lowest level at different stress levels. At low stress level, the other products except Trackless Tack (C) and FastSet exhibit high elastic recovery. However, the percent recovery decreases with the increase of the stress level for all materials. For eTac and eTac-H, the considerable change in percent recovery is observed at higher stress condition. In Figure 11, the J_{nr} increases with the higher stress level. The eTac exhibits the highest J_{nr} at two stress

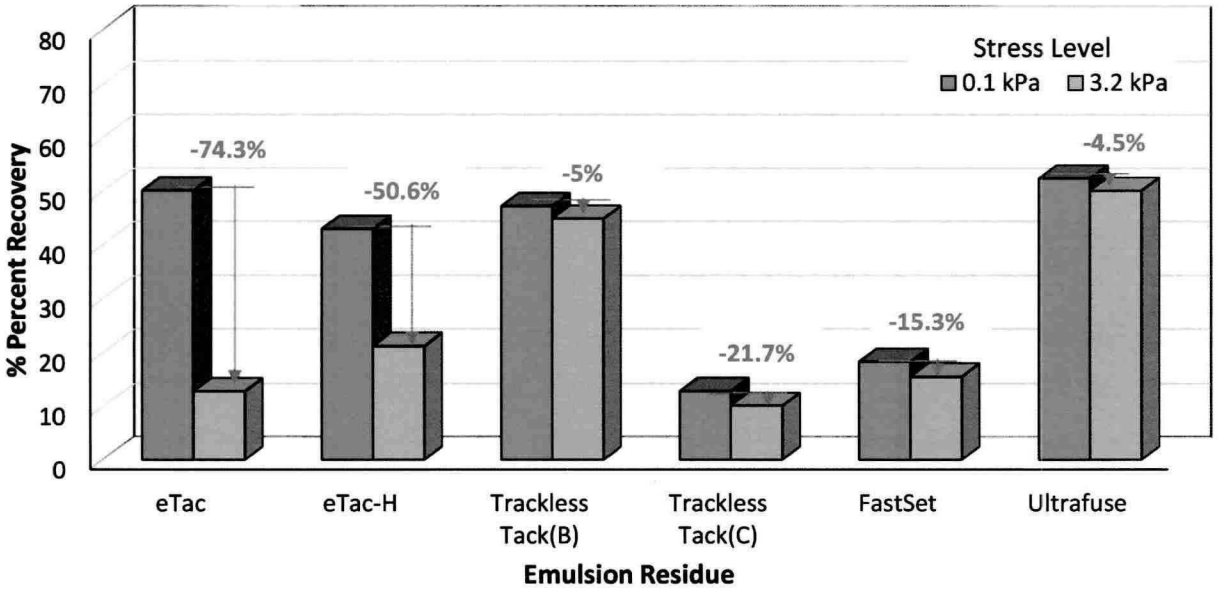

Figure 10. Percent recovery of emulsion residues

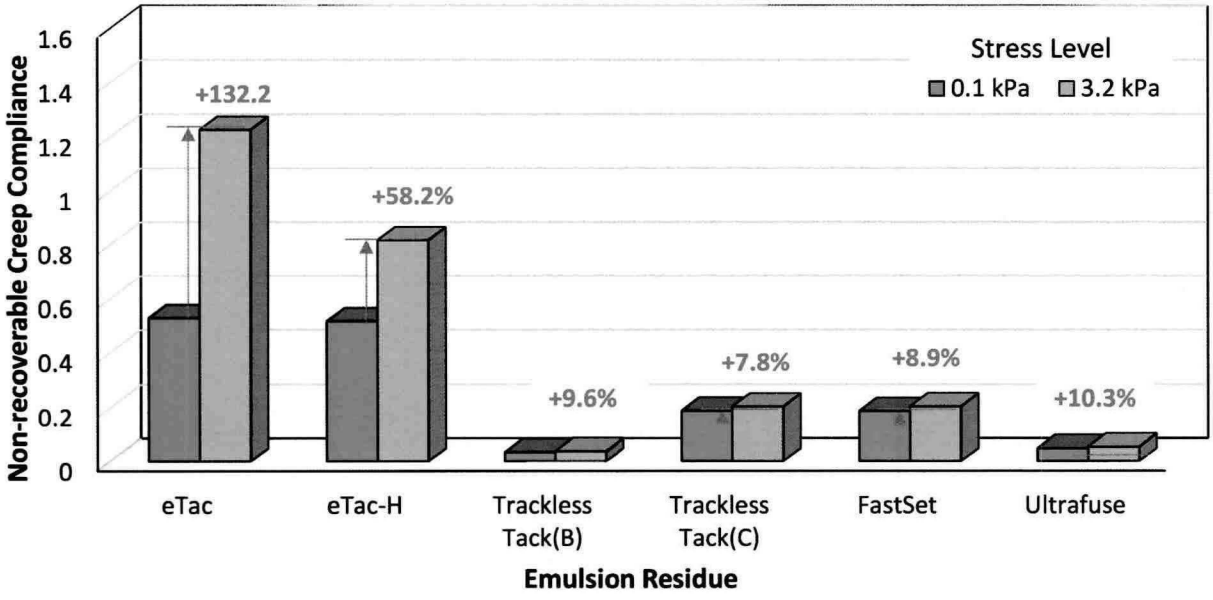

Figure 11. Non-recoverable creep compliance of emulsion residues

levels, following by eTac-H. Also for the residue of these products a dramatic increase in J_{nr} occurs relative to their neat binder. Consequently, there is potential for permanent deformation under high stress conditions for these materials. On the contrary, the other residues are less sensitive to high stress level. Trackless Tack (B) and Ultrafuse exhibit the similar non-recoverable strain response to the stress input. Also, Trackless Tack (C) and FastSet have similar behavior at different stress conditions.

CONCLUSION

The purpose of this task was to characterize non-tracking tacks and a traditional tack using various material properties. Six non-tracking tacks as well as some of their neat binders and one conventional tack were evaluated. The residues were collected after 6 hours of heating using the low temperature evaporative method. The properties and performance of the tacks and tack residues were obtained through three advanced test methods including 1) DSR Frequency Sweep Test, 2) MSCR Test, and 3) LAS Test.

The following are key findings of this task:

- Through DSR frequency sweep test, the residue became stiffer and more elastic than the neat binder over the entire range of frequency. This phenomenon may be caused by the emulsifying and aging process. As frequency decreased, the difference in stiffness between the residue and the neat binder was significant. The residue of the Trackless Tacks manufactured by Blacklidge and Calumet were the stiffest and the most elastic whereas eTac and eTac-H produced by Ergon were the softest and the most viscous.
- The MSCR test showed that the residue exhibited lower J_{nr} and higher percent recovery than the neat binder. Aging and emulsification also led to the change in J_{nr} and percent recovery. The Ultrafuse shows the strongest recovery, and the Trackless Tack (C) is the least recovered. The eTac exhibits the highest J_{nr} , and its non-recoverable strain response is the most sensitive to stress level.

Based on these findings, we recommend the following for the remainder of the project work plan:

- Correlate the material properties of tacks to tracking resistance.
- Correlate the physical properties of tacks to bonding strength.
- Complete the LAS test with PAV aged binders to characterize the fatigue resistance.
- Continue to conduct all tests on a conventional tack.
- Run triplicate samples of each test to check the reproductivity.

REFFERENCES

1. Marasteanu, M. O., T. R. Clyne, and A. Basu. Evaluation of Asphalt Binders Used for Emulsions. 2003.
2. Marasteanu, M. O., and D. A. Anderson. Establishing linear viscoelastic conditions for asphalt binders. *Transportation Research Record: Journal of the Transportation Research Board,* Vol. 1728, No. 1, 2000, pp. 1-6.
3. Clyne, T. R., and M. O. Marasteanu. Inventory of properties of Minnesota certified asphalt binders. 2004.
4. Marasteanu, M., and D. Anderson. Improved model for bitumen rheological characterization.In *Eurobitume Workshop on Performance Related Properties for Bituminous Binders*, European Bitumen Association Brussels, Belgium, 1999.
5. Anderson, R. M. Understanding the MSCR Test and its Use in the PG Asphalt Binder Specification. 2011.
6. Hanz, A., Z. Arega, and H. U. Bahia. Rheological Evaluation of Emulsion Residues Recovered Using Newly Proposed Evaporative Techniques.In *Transportation Research Board 88th Annual Meeting*, 2009.
7. Zhou, F., W. Mogawer, H. Li, A. Andriescu, and A. Copeland. Evaluation of Fatigue Tests for Characterizing Asphalt Binders. *Journal of Materials in Civil Engineering,* Vol. 25, No. 5, 2012, pp. 610-617.
8. Mogawer, W., A. Austerman, M. E. Kutay, and F. Zhou. Evaluation of binder elastic recovery on HMA fatigue cracking using continuum damage and overlay test based analyses. *Road Materials and Pavement Design,* Vol. 12, No. 2, 2011, pp. 345-376.
9. Bahia, H. U., D. Hanson, M. Zeng, H. Zhai, M. Khatri, and R. Anderson. *Characterization of modified asphalt binders in superpave mix design*. 2001.
10. Hintz, C., R. Velasquez, C. Johnson, and H. Bahia. Modification and Validation of Linear Amplitude Sweep Test for Binder Fatigue Specification. *Transportation Research Record: Journal of the Transportation Research Board,* Vol. 2207, No. 1, 2011, pp. 99-106.
11. Johnson, C. M. Estimating asphalt binder fatigue resistance using an accelerated test method.In, UNIVERSITY OF WISCONSIN–MADISON, 2010.
12. Schapery, R. A theory of crack initiation and growth in viscoelastic media. *International Journal of Fracture,* Vol. 11, No. 1, 1975, pp. 141-159.
13. Kim, Y., H. Lee, D. Little, and Y. R. Kim. A Simple Testing Method to Evaluate Fatigue Fracture and Damage Performance of Asphalt Mixtures (With Discussion). *Journal of the Association of Asphalt Paving Technologists,* Vol. 75, 2006.